Supporting Information for Influence of vapor wall-loss in laboratory chambers on yields of secondary organic aerosol

Xuan Zhang, Christopher D. Cappa, Shantanu Jathar, Renee C. McVay, Joseph J. Ensberg, Michael J. Kleeman, and John H. Seinfeld

correspondence to: cdcappa@ucdavis.edu or seinfeld@caltech.edu

This file includes:

Section 1. Materials and Methods

The Supplementary information contains an overview of the new and historical chamber experiments (S1.1), optimization of k_w and α (S1.2), the statistical oxidation model (S1.3), the treatment of vapor wall loss within the SOM and a discussion of vapor-particle equilibrium timescales (S1.4), and the fitting of historical chamber data (S1.5).

S1.1. Experiments

S1.1.1. Toluene Photooxidation Experiments

Toluene SOA formation experiments were conducted in the new Caltech dual 24-m^3 Environmental Chambers, in which the temperature (T) and relative humidity (RH) are automatically controlled. Prior to each experiment, the Teflon chambers were flushed with clean, dry air for 24 h until the particle number concentration < 10 cm^{-3} and volume concentration < 0.01 μm^3 cm^{-3}. Ammonium sulfate (AS) seed aerosol was injected into the chamber by atomizing 0.015 or 0.1 M aqueous $(NH_4)_2SO_4$ solution into the chamber for 30 to 120 min. The resulting total AS seed surface area ranged from ~ 1×10^3 μm^2 cm^{-3} up to ~ 1×10^4 μm^2 cm^{-3}, and the corresponding particle-to-wall surface area ratio ranged from ~ 1×10^{-3} to 7×10^{-3}. Hydrogen peroxide (H_2O_2) was used for the OH source by evaporating 120 μL of 50% wt aqueous solution into the chamber with 5 L min^{-1} of purified air for ~ 100 min, resulting in an approximate starting H_2O_2 concentration of 2.0 ppm. 3 μL toluene (Sigma-Aldrich, 99.8% purity) was injected into a glass bulb, which was connected into the Teflon chamber. 5 L min^{-1} of purified air flowed through the glass bulb into the chamber for ~ 15 min, introducing ~ 40 ppb toluene into the chamber. For experiments at elevated NO_x (i.e. high-NO_x conditions) NO and NO_2 were added to the chamber at the start of a given experiment until the concentrations were ~17 ppb and 30 ppb, respectively. The initial [VOC]/[NO_x] in the high-NO_x experiments ranged from 4.8-6.0 ppbC/ppb. After ~ 90 min mixing, photooxidation was initiated by irradiating the chamber with black lights with output wavelength ranging from 300 to 400 nm. The irradiation leads to photolysis of H_2O_2 to produce OH radicals with an approximately constant concentration throughout the entire experiment. Temperature and relative humidity of all experiments were ~298 K and ~3%,

respectively. The initial O_3 concentration was below detection limit in all experiments. H_2O_2 exerts an interference on the O_3 detection, increasing the O_3 monitor readout by ~ 2-3 ppb in the current study. NO was continuously injected into the chamber over the course of each experiment at 80 ppb h^{-1} for the first 2.5 h of reaction, then 50 ppb h^{-1} for the next 4.5 h of reaction, and then 30 ppb h^{-1} for the remainder of the reaction. Experimental conditions (e.g. [VOC], seed surface area, [NO_x]) for each experiment are reported in Table S1.

A suite of instruments was used to monitor toluene SOA formation and evolution. T, RH, NO, NO_x and O_3 were continuously monitored. Toluene concentration was monitored using a gas chromatograph with flame ionization detector (GC/FID, Agilent 6890N), equipped with a HP-5 column (15 m × 0.53 mm ID × 1.5 μm thickness, Hewlett-Packard). Particle size distribution and number concentration were measured by a cylindrical differential mobility analyzer (DMA; TSI Model 3081) coupled to a condensation particle counter (TSI Model 3010). The DMA was operated in a closed system with a recirculating sheath and excess flow of 2.67 L min^{-1} and a 5.4 : 1 ratio of sheath to aerosol flow rate. The column voltage was scanned from 15 to 9850 V over 45 s.

S1.1.2. Historical Experiments

All the other SOA formation experiments used in SOM optimal fitting were carried out in the Caltech dual 28-m^3 Environmental Chamber. Details of experimental protocols can be found in (1-6). Experimental conditions are reported in Tables S2 and S3 and differences in methodology from the above toluene photooxidation experiments are highlighted below. An identical suite of instrumentation was used as in the toluene photooxidation experiments. The historical experiments typically had seed *SA* around 1-2 x 10^3 cm^{-3}, corresponding to the lowest seeded experiments in the toluene photooxidation experiments. The majority of the historical low-NO_x experiments examined in this study used similar methods and conditions as the new toluene experiments, i.e. used H_2O_2 as the OH source. The experimental procedures associated with the high-NO_x experiments differed from the new toluene experiments. Specifically, for the historical high-NO_x experiments the primary OH source was HONO photolysis, as opposed to H_2O_2 photolysis. This has the practical implication of leading to reaction conditions where (i) the OH concentration is initially ~O(10^7 molecules cm^{-3}) and decays rapidly over a period of ~1-3 hours and (ii) the initial [VOC]/[NO_x] ratio tends to be much smaller compared to the current experiments. Thus, the timescales of SOA

formation during the historical high-NO_x experiments were, in general, very different than for the toluene photooxidation experiments: rapid formation over approximately 1-2 hours vs. continuous formation over 18 hours. For high-NO_x experiments, NO_x was added prior to the lights being turned on both from the HONO injection, which introduces some NO_2, and from addition of NO. Additional NO was produced upon photolysis of HONO. Typical initial NO_x concentrations were on the order of 500 ppb, corresponding to initial [VOC]/[NO_x] of ~0.5 ppbC/ppb (Table S3).

S1.1.3. Particle Wall-Loss Correction

Particle wall losses during an experiment must be accounted for. Two limiting assumptions have been made for the interactions between those particles that have deposited on the wall and suspended vapors in determining the corrected suspended SOA concentrations (5, 7, 8). In one case, particles deposited on the wall are assumed to cease interaction with the suspended vapors and no loss of vapors to the walls is accounted for. This case gives the lower bound of the total organic mass concentration, since particles remain the same size as at the moment they deposited on the wall for the remainder of the experiment. SOA concentrations determined from this case are used for the primary analysis in the manuscript, which is appropriate because vapor loss to the walls is treated separately. In the second limiting case, particles deposited on the wall are assumed to continue to interact with the suspended vapors as if they had remained suspended, with the wall-bound particles assumed to grow at the same rate as suspended particles in the chamber. The corrected SOA concentrations in this case are larger than in the first case because of the additional uptake of vapors to wall-bound particles. This case provides an upper-bound on the actual SOA formed under the assumption that the vapors interact with wall-bound particles, but not the Teflon walls (5, 7, 8). However, traditional application of this second case does not account for the substantially differing timescales of gas-particle vs. gas-wall transport, nor does it account for loss of vapors to the chamber walls and the substantially larger amount of effective absorbing mass of the walls (C_w) compared to the deposited particles. Compared with C_w (10 mg m^{-3}), which is assumed as a constant from the onset of the experiment, the total organic mass deposited on the chamber wall over the course of 18 h photooxidation is ~ 3 orders of magnitude lower. As such, this “upper bound” can underestimate the actual SOA formation,

as it accounts for only a subset of the overall vapor wall-loss correction. Nonetheless, the "upper bound" corrected results are provided for reference to previous experiments.

For either case, the Aerosol Parameter Estimation (APE) model (9), derived on the basis of the aerosol general dynamic equation (10), is employed to calculate these two limits. The suspended particle population evolves as a result of three processes: coagulation, condensation, and wall-loss. The change of suspended particle number-size distribution due to coagulation is well constrained. The size-dependent wall loss rate is determined by experimentally monitoring the decay of dry inert $(NH_4)_2SO_4$ particles assuming first-order kinetics. The condensation rate is the only free parameter in the model, which can be obtained by optimal fitting of the APE model predictions to the DMA measured particle size distribution at each time step. Once the condensation rate values are estimated, they can be applied to parameterize the growth of particles on the walls due to condensation of gaseous vapor and deposition of suspended particles. A factor that describes the extent of interactions between deposited particles and suspended vapors is applied when summing aerosol masses in the chamber core and on the walls. A value of 0 for this factor corresponds to no condensation to deposited particles. A value of 1 for this factor corresponds to the case where the condensation rate of gaseous vapors to deposited particles is the same as those suspended. The primary analysis in this work utilizes the corrected particle mass under the assumption of no condensation to deposited particles because vapor wall loss is treated separately. The evolution of the wall-loss corrected particle size distributions is shown for each experiment in Fig. S1 for the lower limit case. The time-dependent aerosol growth, from which the aerosol yield can be calculated, is shown for each experiment in Fig. S2 for both limiting cases.

S1.2. Optimizing k_w and α

The optimal values of k_w and α were determined using the general procedure as outlined below. There were a total of 6 experiments conducted for each NO_x condition, 5 with seed aerosol and 1 without. Only the seeded experiments are considered in the optimization method because of difficulties associated with specification of nucleation. The SOM was fit to one of these 5 seeded experiments for a variety of k_w and α values. For each k_w/α pair a set of best-fit SOM parameters (i.e. ΔLVP, m_{frag} and the P_{func} array) were determined. Specifically,

the experiments with seed SA = 5.5 x 10^3 μm^2 cm^{-3} (low-NO_x) and SA = 3.5 x 10^3 μm^2 cm^{-3} (high-NO_x) were used for fitting. These best-fit SOM parameters and the associated k_w/α pair were then used to simulate SOA formation for the other 4 seeded experiments. Reduced goodness of fit metric (χ^2_{red}) values were calculated for each experiment as:

$$\chi^2_{red} = \frac{1}{n-6-1}\sum\left(\frac{C_{OA,obs}(t)-C_{OA,model}(t)}{\sigma_{OA,obs}(t)}\right)^2 \quad \text{(S1)}$$

where n is the number of data points per experiment, 6 is the number of model degrees of freedom and $\sigma_{OA,obs}$ is the uncertainty in the observations. For each experiment, the minimum χ^2_{red} across all k_w/α pairs was determined, and the set of χ^2_{red} values for each experiment was normalized by the minimum in that set. Normalization ensures that the different experiments carry equal weight in the next step. The composite χ^2_{red} across all seeded experiments was then determined as:

$$\chi^2_{red,composite}(k_w,\alpha) = \sum_{i=1}^{5}\chi^2_{red,norm,i}(k_w,\alpha) \quad \text{(S2)}$$

where the sum is over the normalized χ^2_{red} for all seeded experiments. Smaller values of the composite χ^2_{red} indicate overall better agreement across all of the seeded experiments for a given set of best-fit SOM parameters, k_w and α. A contour diagram of the calculated composite χ^2_{red} as a function of k_w and α (Fig. S3) illustrates that only certain combinations of k_w and α provide for good agreement across all experiments. There is almost no seed effect when $\alpha > 0.1$, and therefore the overall agreement is poor no matter what k_w is used. As α is lowered, a seed effect becomes evident. However, only when α is O(10^{-3}) and k_w is O(10^{-4}) can overall good agreement with all experiments be obtained. Since the k_w and α values were not determined from a specific fitting algorithm, we refer to the values that provide for best agreement as the "optimal" values rather than "best fit" values. These are: k_w = 2.5 x 10^{-4} s^{-1} and α = 2 x 10^{-3} for low-NO_x experiments and k_w = 2.5 x 10^{-4} s^{-1} and α = 1 x 10^{-3} for high-NO_x experiments.

S1.3. The Statistical Oxidation Model

The SOM simulates the oxidation of a given hydrocarbon as a trajectory through a 2-D grid of carbon and oxygen atoms in which "species" are considered particular carbon/oxygen combinations (e.g. $C_{12}O_4$). Specific rules define the movement through this space, describing the probability that a reaction leads to functionalization or fragmentation, how many oxygen atoms are added per reaction, and the decrease in vapor pressure that occurs upon addition of a single oxygen atom. SOM effectively simulates the multi-generational chemistry that characterizes photooxidation experiments. Full details are provided in (6, 11). The fragmentation probability (P_{frag}) depends on the oxygen content of the reacting species and is parameterized as:

$$P_{frag} = \left(\frac{N_O}{N_C}\right)^{m_{frag}} \quad \text{(S3)}$$

where m_{frag} is an adjustable parameter, and N_O and N_C are the number of oxygen and carbon atoms comprising an SOM species, respectively. The P_{frag} is always constrained to be ≤ 1. (Recently, a "bug" in the SOM code was found related to how the fragmentation was being treated. Rather than the probability of fragmentation depending on the oxygen content of the reacting species, it was being determined based on the oxygen content of the product species. This has now been fixed. The SOM was originally written in the IGOR programming language. The SOM has now been independently implemented in Fortan using the framework outlined in (11) and the IGOR and Fortan versions produce equivalent results, suggesting that no further "bugs" of this sort exist. The best-fit SOM parameters for the alkanes differ from those reported in (6) as a result of this update and because vapor wall-loss has been included.)

The functionalization probability (P_{func}) describes the likelihood of adding 1, 2, 3 or 4 oxygen atoms per reaction, and each can be adjusted independently, subject to the constraint that they are positive and must sum to 1. The decrease in vapor pressure (or more specifically, in the log of the saturation concentration, C^*, in μg m^{-3}) per oxygen added is referred to as ΔLVP, and ranges from ~0.7 to 2.5, depending on the type of functional group added. Thus, there are

194 6 total adjustable (tunable) parameters in the base model: (i) fragmentation, (ii) volatility
195 decrease per oxygen added and (iii-vi) oxygen addition probability. For this study,
196 heterogeneous OH reactions are not simulated.

197 The reaction rate coefficient matrix associated with reactions of product species with OH
198 radicals has been updated from the original SOM on the basis of comparison with output from
199 the GECKO-A model for simulations of the outflow from Mexico City (12). The reaction rate
200 coefficient of the parent hydrocarbon with OH, k_{OH} (cm^3 $molecules^{-1}$ s^{-1}), is specified to be
201 consistent with literature results, e.g. for toluene k_{OH} = 5.2 x 10^{-12} cm^3 $molecules^{-1}$ s^{-1}. For all
202 other species within the SOM grid, the k_{OH} are determined referenced to the reaction rate
203 coefficient for species with the same number of carbon atoms but zero oxygen atoms as:

204

205 $$\log\left(k_{OH,base}\right) = A_1 + A_2 \times N_C^{A_3} \quad \text{(S4)}$$

206

207 and where A_1 = -15.103, A_2 =-3.9481, and A_3 = -0.79796. For a given N_C, the k_{OH} is
208 temperature dependent and varies with N_O as

209

210 $$k_{OH}(T) = k_{OH,base} \times T^2 \times exp\left(-1 \times \frac{E_a}{8.314 \times T}\right) \times \left[1 + \frac{b_1}{\sigma\sqrt{2\pi}} \exp\left(-\frac{1(ln(N_O+0.01)-ln(b_2))^2}{2\sigma^2}\right)\right]$$

211 (S5)

212 and where the variables b_1, b_2, and σ are functions of N_C, with

213

214 $$\sigma(N_C \leq 15) = 0.0214 \times N_C + 0.5238; \;\; \sigma(N_C > 15) = -0.115 \times N_C + 2.695 \text{ ,} \quad \text{(S6)}$$

215

216 $$b_1 = -0.2583 \times N_C + 5.8944 \text{ ,} \quad \text{(S7)}$$

217

218 And

219

$$b_2(N_C \leq 15) = 0.0314 \times N_C + 0.9871\,;\, b_2(N_C > 15) = 0.25 \times N_C - 2.183\,. \quad \text{(S8)}$$

Within the SOM gas-particle partitioning is treated through the framework of absorptive partitioning theory (13), in which compounds partition between the gas and particle phases according to their Raoult's Law adjusted vapour pressures. Unlike in previous usages of the SOM, which assumed instantaneous gas-particle equilibrium, the SOM here treats gas-particle mass transfer dynamically. The net flux of molecules to/from the particle is calculated at each timestep as:

$$\frac{\partial C_{OA,i}}{dt} = 4\pi D_{gas,i} R_p N_p F_{FS}\left(C^{\infty}_{gas,i} - \chi_i C^*_i\right) \quad \text{(S9)}$$

where $D_{\mathrm{gas,i}}$ is the gas-phase diffusivity, R_{p} is particle radius, N_{p} is particle number concentration, F_{FS} is the Fuchs-Sutugin correction for noncontinuum mass transfer, $C^{\infty}_{gas,i}$ is the gas-phase concentration, χ_{i} is the mass fraction and C^*_i is the saturation concentration of species *i*. The entire SOA mass is considered absorbing in the calculation of χ_{i}. It is assumed that $D_{\mathrm{gas,i}}$ varies with molecular weight (*MW*) and is equal to $D_{\mathrm{CO2}}(\mathrm{MW_{CO2}}/\mathrm{MW_i})$, with D_{CO2} = 1.38 x 10^{-5} $\mathrm{m^2\ s^{-1}}$. The Fuchs-Sutugin correction is equal to:

$$F_{FS} = \frac{0.75\alpha(1+Kn)}{Kn^2+Kn+0.283\cdot Kn\cdot\alpha+0.75\alpha} \quad \text{(S10)}$$

where α is the mass accommodation coefficient onto particles and *Kn* is the Knudsen number, defined as:

$$Kn = \lambda / R_p \quad \text{(S11)}$$

and λ is the gas mean free path, which is equal to:

$$\lambda_i = 3 \cdot \frac{D_{gas,i}}{\bar{c}_i} \quad \text{(S12)}$$

with $\bar{c}_i$ equal to the root mean square speed of the gas, which is equal to:

$$\bar{c}_i = \left(\frac{8N_A kT}{\pi MW_i}\right)^{\frac{1}{2}} \quad \text{(S13)}$$

with N_A = Avagadro's number, k = the Boltzmann constant and T = temperature. The results obtained with the dynamic partitioning SOM are equivalent to those obtained using the instantaneous equilibrium assumption when $\alpha > 0.1$ and with seed aerosols present. It should be noted that α as used in Eqn. S8 represents the net mass transfer and can include resistances both in the gas-phase and at the particles surface. Full accommodation of vapors into the bulk particle can be limited by diffusion within the particles when particles are highly viscous (14). The dynamic SOM utilized here uses monodisperse particles with a size equal to the number mean diameter and the number concentration adjusted to give the desired initial seed surface area (*SA*). Although the ideal model would use the actual seed size distribution as input, we have established that for particle diameters larger than ~ 50 nm the model results are sufficiently insensitive to the selected particle diameter for a fixed seed *SA*. As such, the results here are not limited by the simplification of using monodisperse particles. Nucleation is not explicitly simulated by the SOM. Therefore, dynamic SOM calculations for the nucleation experiments have been carried out assuming an initial seed size of 5 nm and a seed concentration equal to that observed at the end of the experiment. Given that there is substantial uncertainty associated with this assumption the nucleation experiments have not been quantitatively assessed.

S1.4. Vapor Wall-Loss

Loss of vapors to the chamber walls is simulated as a first-order process, characterized by the first-order wall-loss coefficient k_w (s^{-1}). Vapor wall-losses are assumed to be reversible, characterized by the gas-wall partitioning coefficient, K_w, which is dependent upon compound vapor pressure,

$$K_w = \frac{RT}{M_w \gamma_w P_{sat}} \quad \text{(S14)}$$

where R is the ideal gas constant, T is temperature (assumed 298 K), M_w is the effective molecular weight of the wall material, γ_w is the activity coefficient, and P_{sat} is the saturation concentration of the species of interest. It is convenient to use the saturation concentration, C^* (μg m^{-3}), instead of the saturation vapor pressure, where

$$C^* = \frac{1}{K_p} = \frac{M_p \gamma_p P_{sat}}{RT} \quad \text{(S15)}$$

with K_p the gas-particle partitioning coefficient, M_p the average molecular weight of the organic species comprising the particles and γ_p is the activity coefficient. The rate coefficient for transfer of gas-phase species onto the walls is given as $k_{w,on}$ while that for evaporation from the walls is given as $k_{w,off}$. The $k_{w,on}$ is specified as a model input parameter (and is equivalent to the k_w in the main text). The $k_{w,off}$ is obtained from detailed balance as:

$$k_{w,off} = \frac{k_{w,on}}{K_w C_w} = k_{w,on}\left(\frac{C^* M_w \gamma_w}{C_w M_p \gamma_p}\right) \quad \text{(S16)}$$

and where C_w is the equivalent wall OA concentration (μg m^{-3}). If one makes the simple assumption that $M_w = M_p$ and $\gamma_w = \gamma_p$, then C_w can be viewed as an effective concentration that accounts for differences in molecular weight and activity between the particles and walls.

297 The C_w must therefore be estimated from experiments. Matsunaga and Ziemann (15) report a
298 range of C_w values that are constant within a given class of molecules (e.g. ketones vs.
299 alkanes), with C_w = 2, 4, 10 and 24 mg m^{-3} for alkanes, alkenes, alcohols and ketones. For all
300 reported simulations here it has been assumed that C_w = 10 mg m^{-3}. Results are reasonably
301 insensitive to the choice of C_w over the previously determined range because $C_w >> C_{OA}$. The
302 sensitivity of our results to the assumed C_w is discussed further below in Section S1.4.3.

303 It is assumed that $k_{w,on}$ is not dependent on compound identity. Consequently, the $k_{w,off}$ terms
304 vary with compound identity, specifically with C^*.

305 The value of $k_{w,on}$ can be estimated from consideration of just the gas-phase transport terms
306 within a chamber. McMurry and Grosjean (16) report an expression for $k_{w,on}$,

307

308 $$k_{w,on} = \left(\frac{A}{V}\right)\frac{\left(\frac{\alpha_w \bar{c}}{4}\right)}{1.0+\left(\frac{\pi}{2}\right)\left[\frac{\alpha_w \bar{c}}{4\left(k_e D_{gas}\right)^{0.5}}\right]} \quad \text{(S17)}$$

309

310 where A/V is the surface to volume ratio of the chamber (equal to $6/L$ for a square chamber,
311 and where L is the length of one side), α_w is the mass accommodation coefficient of vapors
312 onto the chamber walls, $\bar{c}$ is the mean thermal speed of the molecules, k_e is the coefficient of
313 eddy diffusion, and D_{gas} is the molecular diffusivity. It should be noted that α_w is not
314 necessarily equal to α for uptake onto particles. For the type of molecules here, D_{gas} is ~3 x
315 10^{-6} m^2 s^{-1} and $\bar{c}$ ~ 200 m s^{-1}. This leaves k_e and α_w as the two key unknowns. Values of $k_{w,on}$
316 have been calculated as a function of k_e for α_w ranging from 10^{-7} to 1, where 1 is perfect
317 accommodation. k_e values from 10^{-3} s^{-1} to 1 s^{-1} have been used, which corresponds to mixing
318 timescales of 17 min to 1 s (Fig. S4). McMurry and Grosjean (16) reported values for their
319 actively mixed chambers of 0.02 s^{-1} (60 m^3 chamber) and 0.12 s^{-1} (4 m^{-3} chamber). Since the
320 Caltech chamber is not actively mixed it is expected that the characteristic k_e value is
321 considerably smaller.

322 The value of k_e for the Caltech chamber is estimated based on observed size-dependent
323 deposition rates of particles in the chamber. The minimum in the k_w for particles as a function
324 of size is dependent upon k_e. This minimum occurs at a diameter of ~350 nm for the 24 m^{-3}

Caltech chamber and at ~250 nm for the 28 m^{-3} chamber (5). For particles in a cubic chamber the k_w is related to the eddy diffusion coefficient through the equation (17):

$$k_w = \frac{1}{L}\left[\frac{8\sqrt{k_e D}}{\pi} + v \cdot \coth\left(\frac{x}{2}\right)\right] \quad \text{(S18)}$$

where v is the particle terminal settling velocity (m s^{-1}) and x is defined as:

$$x = \frac{\pi v}{2\sqrt{k_e D}} \quad \text{(S19)}$$

From Eqn. S5, k_w has been calculated as a function of particle diameter and the k_e value adjusted until the minimum occurs at 250 nm or 350 nm. The required k_e in the 24 m^3 chamber is 0.075 s^{-1} and in the 28 m^3 chamber is 0.015 s^{-1}, similar to the values reported by McMurry and Grosjean for 60 m^3 (k_e = 0.12 s^{-1}) and 4 m^3 (k_e = 0.02 s^{-1}) chambers (16). Therefore, it is expected that the *maximum* k_w ~ 6.0 x 10^{-4} s^{-1} for the 24 m^3 chamber and ~ 3 x 10^{-4} for the 28 m^3 chamber from consideration of Fig. S4. Since the accommodation coefficient for the condensing species on the Teflon chamber walls is not known, it is not possible to definitively put a lower bound on the k_w. However, the experimental results of Matsunaga and Ziemann (15) clearly demonstrate that vapors are taken up to their chamber walls quite rapidly, and they estimate that $\alpha_w \sim 10^{-5}$, which suggests that k_w ~ 3 x 10^{-4} s^{-1} (24 m^3) or ~ 2 x 10^{-4} s^{-1} (28 m^3). This theoretical estimate is in very good agreement with the optimal k_w (= 2 x 10^{-4} s^{-1}) for the 24 m^3 chamber.

Loza et al. (18) report observations of vapor wall-loss rates for two compounds: 2,3-epoxy-1,4-butanediol (BEPOX) and glyoxal. BEPOX is the butadiene derivative of an epoxydiol of isoprene. The uptake of both compounds to the chamber walls was observed to depend strongly on RH and whether a "new" or "old" chamber was used, with the measured values ranging from ~2-7 x 10^{-5} s^{-1} (18). Such new vs. old dependence was not observed by Matsunaga and Ziemann (15), who investigated wall-losses of alkanes, alkenes, 2-ketones and 2-alcohols. This suggests that the mechanism involved in the uptake of BEPOX and glyoxal

was somewhat different than that for the hydrocarbons considered by Matsunaga and Ziemann (15), or may alternatively indicate complications associated with capturing fast initial decay during the fill period in the much larger Caltech chamber. Such fill and mixing complications likely also explain the strong differences between the wall-loss rate coefficients for 2-dodecanol determined by Loza et al. (19) and Matsunaga and Ziemann (15). Since the vapor uptake to the Teflon chamber walls is reversible, care must be taken in the interpretation of observed wall-loss rates. Only measurements made in the very early stages of uptake will correspond directly to the first-order wall-loss rate coefficient, since as the system approaches equilibrium net vapor uptake will slow. As such, we suggest that the estimates of k_w using the α from Matsunaga and Ziemann (15) may be more relevant to the current study given the nature of the compounds involved.

S1.4.1. Gas-Particle Partitioning Timescales

The timescale associated with reaching gas-particle equilibrium varies with seed *SA*, and for a distribution is approximately:

$$\tau_{g-p} \sim \left(2\pi N_p \overline{D_p} D_{gas} \bar{F}_{FS}\right)^{-1} \quad \text{(S20)}$$

where N_p is the particle number concentration, $\overline{D_p}$ is the number mean diameter, D_{gas} is the gas-phase diffusivity and $\bar{F}_{FS}$ is the correction to the mass transfer flux due to noncontinuum effects and imperfect accommodation given in Eqn. S8. Values for τ_{g-p} have been calculated for the low-NO_x experiments based on the initial seed number concentration and mean diameter as a function of α (Fig. S5), using D_{gas} = 1 x 10^{-5} m^2 s^{-1} and λ = 150 nm. The τ_{g-p} vary approximately inversely with α. The optimal α was determined to be $\alpha \sim 0.002$, corresponding to an optimal k_w = 2 x 10^{-4} s^{-1}, or a lifetime with respect to wall loss of $\tau_w = 1/k_w$ = 83 min. The τ_{g-p} for the experiment with the smallest seed concentration (1.4 x 10^3 μm^2 cm^{-3}) when α = 0.001 is 230 min, very similar to τ_w. As seed *SA* increases, the τ_{g-p} decrease to ~30 min for the highest seed *SA*. This difference in the relative values of τ_{g-p} vs. τ_w explains why the seed effect is seen most strongly when seed *SA* is less than ~ 3 x 10^3 μm^2 cm^{-3}, because this is the point at which the two timescales become highly competitive. Similarly, it

helps to explain why larger values of α do not lead to a noticeable seed *SA* dependence; when $\alpha > 0.1$ the $\tau_{g\text{-}p} = 2$ min for the experiment with the smallest seed *SA*.

S1.4.2. Dependence on VOC and OH concentrations

Calculations were performed to determine the magnitude of the wall-loss bias (R_{wall}) as a function of the initial [toluene] and [OH] based on the best-fit of the SOM to the low-NO_x set of experiments. Fig. S6 shows the variation in the end of experiment SOA concentration as a function of initial toluene and OH, and corresponds to the results shown in Fig. 3 in the main text.

S1.4.3. Sensitivity to C_w

As discussed in the main text, the sensitivity of our results to the assumed C_w is has been established by performing fits to the observations for varying values of C_w, from 0.01 to 10 mg m^{-3} for the suite of low-NO_x toluene photooxidation experiments (c.f. Fig. 4). Here, it was assumed that $k_w = 2 \times 10^{-4}$ s^{-1} and $\alpha = 2 \times 10^{-3}$, consistent with the optimized values determined in the main text. Good fits are obtained over the entire range of C_w. Above C_w = 0.2 mg m^{-3} (= 200 μg m^{-3}) the calculated wall-loss bias, R_{wall}, is constant. Below 0.2 mg m^{-3} the calculated R_{wall} falls off, reaching a second plateau at small C_w that is still above unity. The best-fit SOM parameters vary systematically with C_w (Fig. S7), apparently compensating for the varying levels of vapor wall-loss.

S1.5. Fitting of Historical Chamber Data

Beyond the toluene experiments, which are the focus of the manuscript, best-fit SOM parameters have been determined for a suite of historical photooxidation experiments conducted using a variety of other precursor compounds, both under low- and high-NO_x conditions. The historical experiments were all carried out in the prior 28 m^3 Caltech chamber. Experimental conditions are given in Tables S2 and S3. Fitting of the SOM to the observations is performed for these experiments assuming that $k_w = 1 \times 10^{-4}$ s^{-1}, $\alpha = 2 \times 10^{-3}$ and $C_w = 10$ mg m^{-3}. The results are relatively insensitive to C_w when varied over the range 2-24 mg m^{-3}, as discussed above. The value of k_w for the historical chamber is estimated to be slightly smaller than the optimal value determined for the new 24 m^3 chamber based on

411 consideration of the size-dependent particle wall-loss rates, as discussed in Section S1.4. Best
412 fit SOM parameters for low-NO_x and high-NO_x conditions are given in Table S4. Wall-loss
413 bias values were calculated in the same manner as for the toluene experiments. Experimental
414 data and simulation results are shown in Fig. S8-9.

415

416 S1.6. References

417 1. Chan AWH*, et al.* (2009) Secondary organic aerosol formation from photooxidation
418 of naphthalene and alkylnaphthalenes: implications for oxidation of intermediate
419 volatility organic compounds (IVOCs). *Atmos. Chem. Phys.* 9(9):3049-3060.

420 2. Chhabra PS, Flagan RC, & Seinfeld JH (2010) Elemental analysis of chamber organic
421 aerosol using an aerodyne high-resolution aerosol mass spectrometer. *Atmos. Chem.*
422 *Phys.* 10(9):4111-4131.

423 3. Ng NL*, et al.* (2007) Secondary organic aerosol formation from m-xylene, toluene,
424 and benzene. *Atmos. Chem. Phys.* 7(14):3909-3922.

425 4. Chhabra PS*, et al.* (2011) Elemental composition and oxidation of chamber organic
426 aerosol. *Atmos. Chem. Phys.* 11(17):8827-8845.

427 5. Loza CL*, et al.* (2012) Chemical aging of m-xylene secondary organic aerosol:
428 laboratory chamber study. *Atmos. Chem. Phys.* 12(1):151-167.

429 6. Cappa CD*, et al.* (2013) Application of the Statistical Oxidation Model (SOM) to
430 secondary organic aerosol formation from photooxidation of C12 Alkanes. *Atmos.*
431 *Chem. Phys.* 13:1591-1606.

432 7. Hildebrandt L, Donahue NM, & Pandis SN (2009) High formation of secondary
433 organic aerosol from the photo-oxidation of toluene. *Atmos. Chem. Phys.* 9(9):2973-
434 2986.

435 8. Weitkamp EA, Sage AM, Pierce JR, Donahue NM, & Robinson AL (2007) Organic
436 aerosol formation from photochemical oxidation of diesel exhaust in a smog chamber.
437 *Environmental Science & Technology* 41(20):6969-6975.

438 9. Pierce JR*, et al.* (2008) Constraining Particle Evolution from Wall Losses,
439 Coagulation, and Condensation-Evaporation in Smog-Chamber Experiments: Optimal
440 Estimation Based on Size Distribution Measurements. *Aerosol Science and*
441 *Technology* 42(12):1001-1015.

442 10. Seinfeld, J. H. and Pandis, S. N.: Atmospheric chemistry and physics: From air
443 pollution to climate change, Wiley, New Jersey, 612pp., 2006

444 11. Cappa CD & Wilson KR (2012) Multi-generation gas-phase oxidation, equilibrium
445 partitioning, and the formation and evolution of secondary organic aerosol. *Atmos.*
446 *Chem. Phys.* 12:9505-9528.

12. Lee-Taylor J, *et al.* (2011) Explicit modeling of organic chemistry and secondary organic aerosol partitioning for Mexico City and its outflow plume. *Atmospheric Chemistry and Physics* 11(24):13219-13241.

13. Pankow JF (1994) An absorption-model of the gas aerosol partitioning involved in the formation of secondary organic aerosol. *Atmos. Environ.* 28(2):189-193.

14. Shiraiwa M, *et al.* (2013) Size distribution dynamics reveal particle-phase chemistry in organic aerosol formation. *Proc. Nat. Acad. Sci.*

15. Matsunaga A & Ziemann PJ (2010) Gas-Wall Partitioning of Organic Compounds in a Teflon Film Chamber and Potential Effects on Reaction Product and Aerosol Yield Measurements. *Aerosol Sci. Technol.* 44(10):881-892.

16. McMurry PH & Grosjean D (1985) Gas and aerosol wall losses in Teflon film smog chambers. *Environ. Sci. Technol.* 19(12):1176-1182.

17. Crump JG & Seinfeld JH (1981) Turbulent deposition and gravitational sedimentation of an aerosol in a vessel of arbitrary shape. *J Aerosol Sci* 12(5):405-415.

18. Loza CL, *et al.* (2010) Characterization of Vapor Wall Loss in Laboratory Chambers. *Environ. Sci. Technol.* 44(13):5074-5078.

19. Loza CL, *et al.* (2013) Secondary organic aerosol yields of 12-carbon alkanes. *Atmos. Chem. Phys. Discuss.* 13(8):20677-20727.

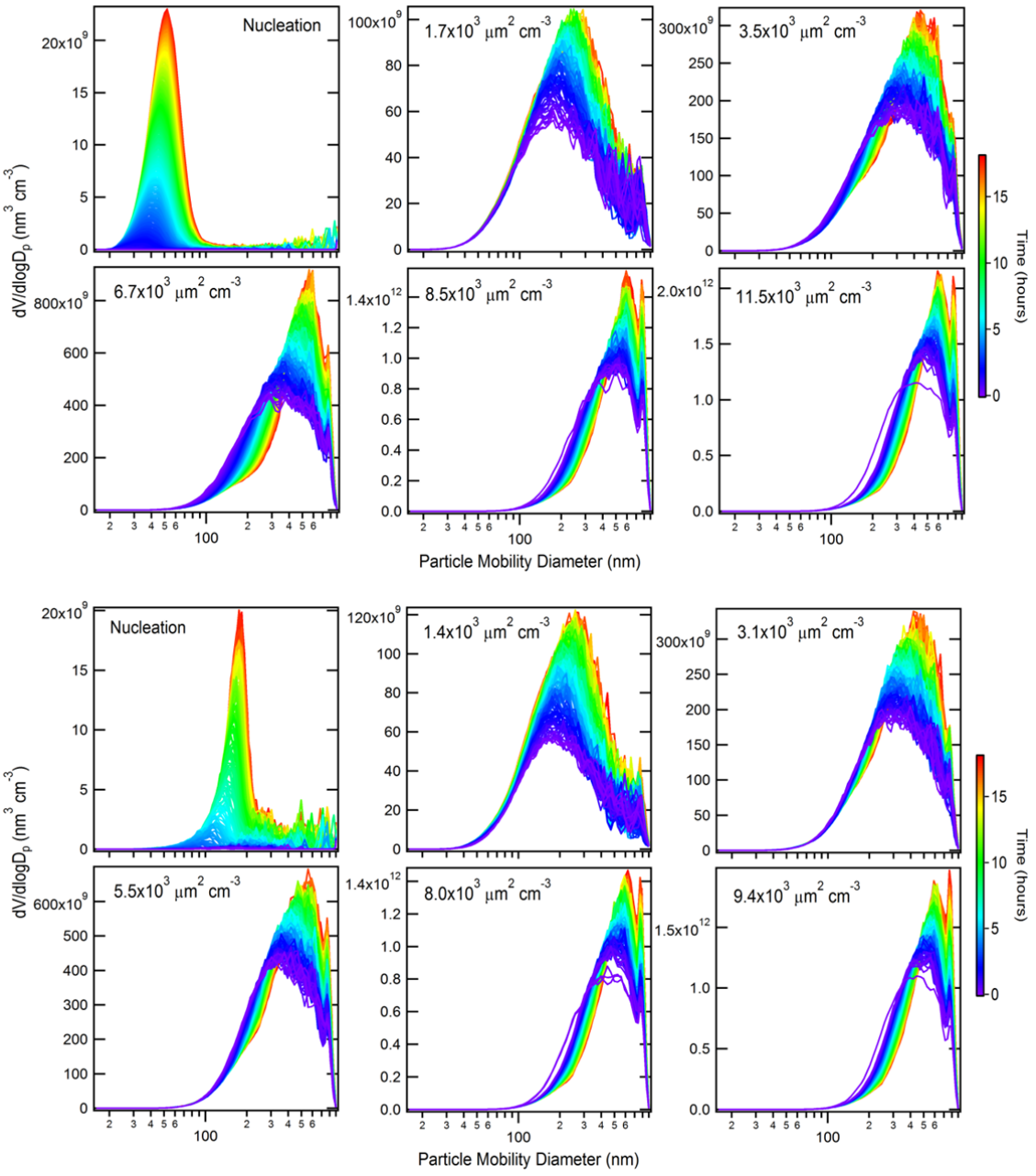

Fig. S1: Time-dependent volume distributions ($dV/dlogD_p$) of AS seed and organic aerosols after 0 - 18 h of photoxidation of toluene under (top panels) high-NO_x and (bottom panels) low-NO_x conditions. Distributions are colored according to the time after lights were turned on. The lower bound wall-loss correction is used here. For the experiments at higher seed *SA*, the influence of coagulation on the particle evolution is evident.

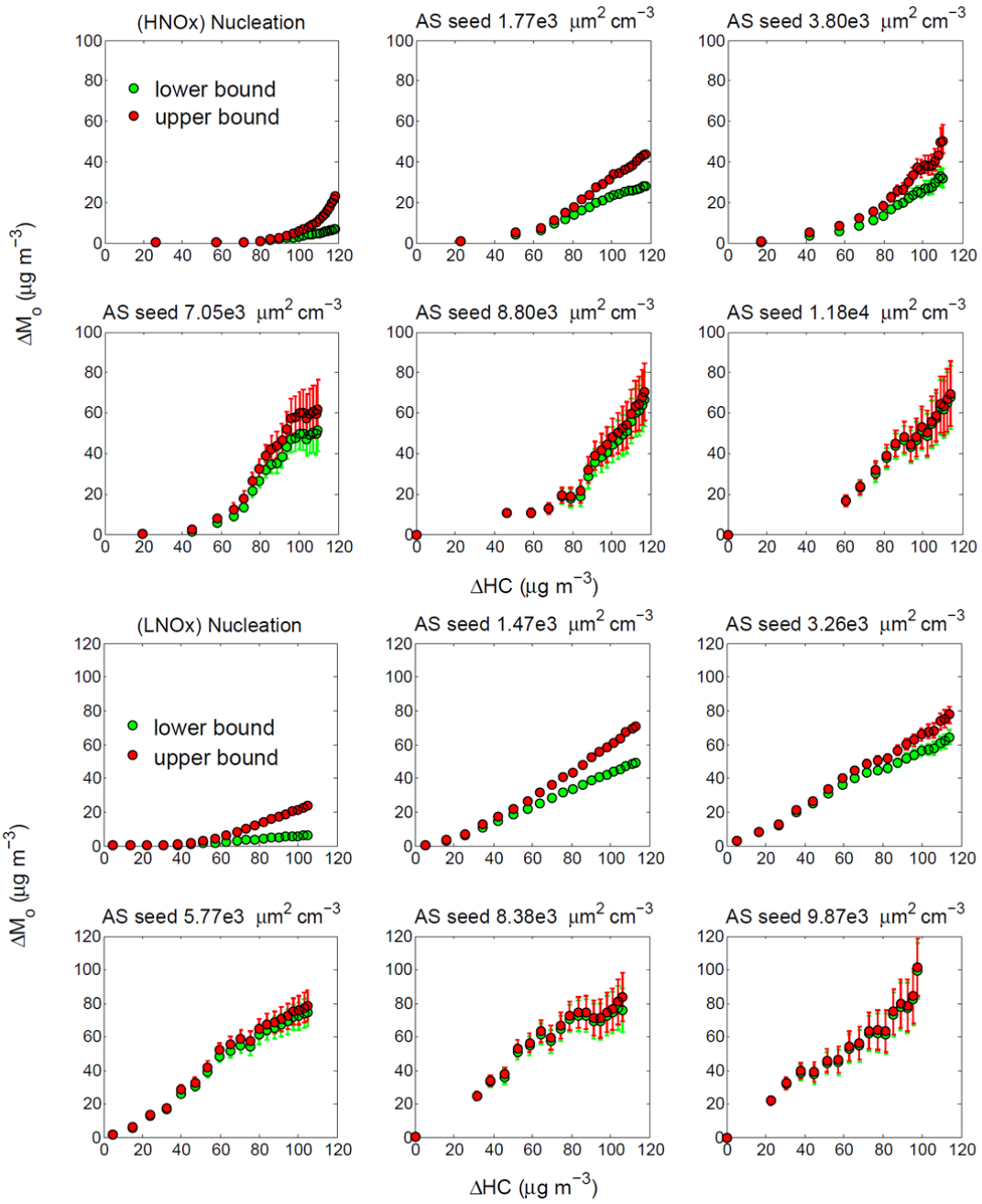

Fig. S2: Time-dependent SOA growth curves for toluene photooxidation under high-NO_x (HNO_x) and low-NO_x (LNO_x) conditions. Error bars come from the 95% confidence interval associated with determining the size-dependent first-order wall-loss rate for dry inert ammonium sulfate ($(NH_4)_2SO_4$) particles.

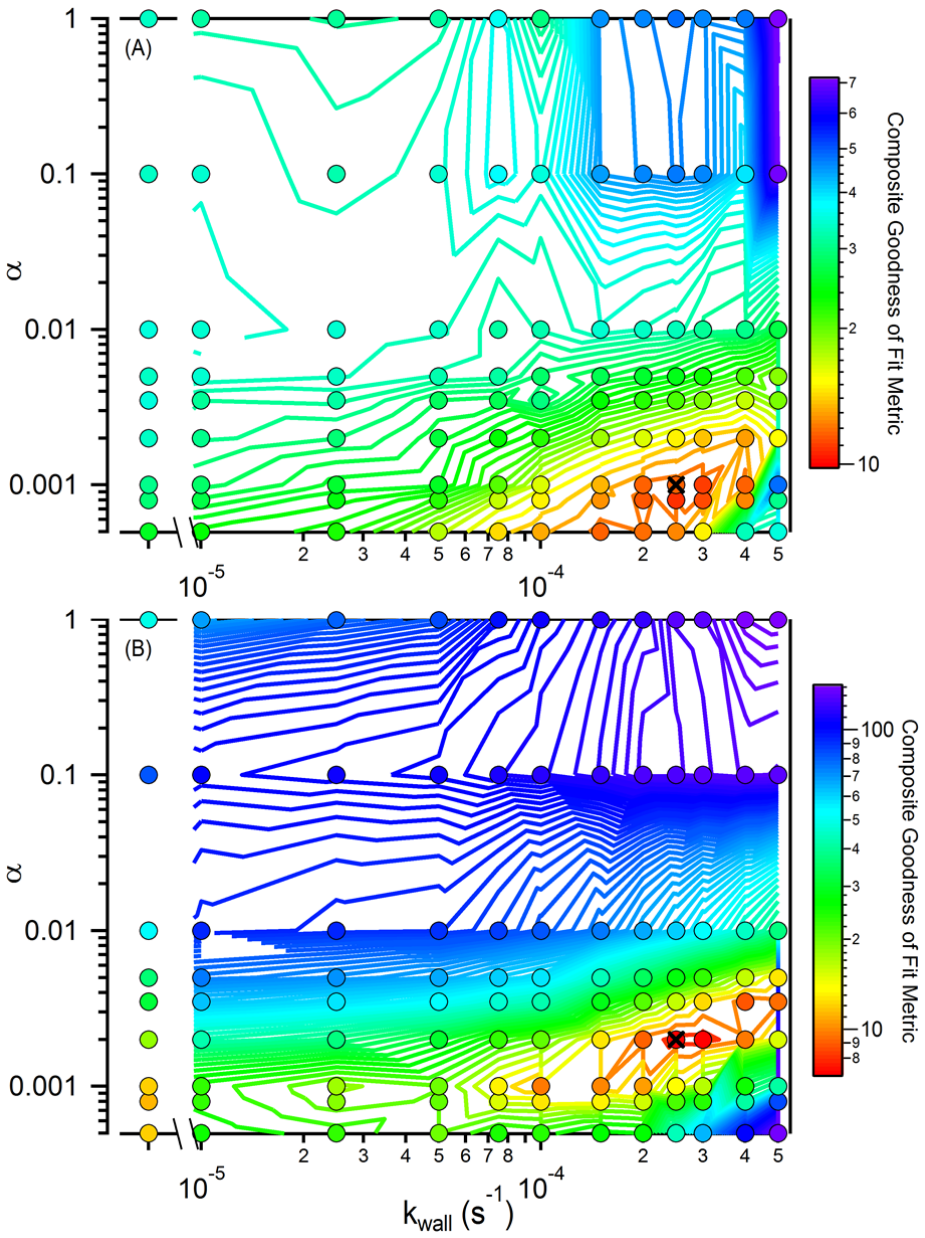

Fig. S3: Calculated composite reduced chi-square values for (A) high-NO_x and (B) low-NO_x toluene experiments as a function of the mass accommodation coefficient, α, and the first order wall-loss rate coefficient, k_w. The colors indicate the magnitude of the calculated composite reduced goodness of fit metric, with the contours based on the circles. The black x indicates the optimal value: $k_w = 2.5 \times 10^{-4}$ s^{-1} and $\alpha = 1 \times 10^{-3}$ (high-NO_x) and $k_w = 2.5 \times 10^{-4}$ s^{-1} and $\alpha = 2 \times 10^{-3}$ (low-NO_x).

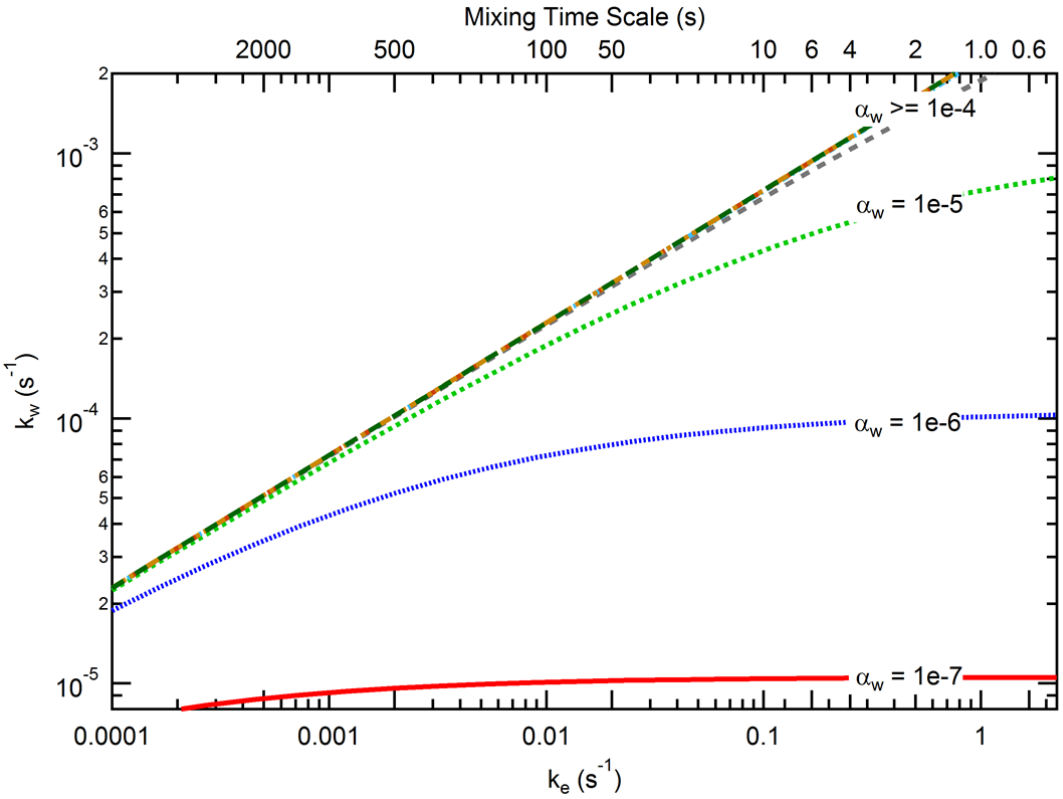

Fig. S4: Calculated wall-loss coefficients k_w as a function of the coefficient of eddy diffusion, k_e, which characterizes the state of turbulent diffusion in the chamber, for different values of the mass accommodation coefficient onto the walls, α_w. The top axis shows the time-scales corresponding to the eddy diffusion coefficients.

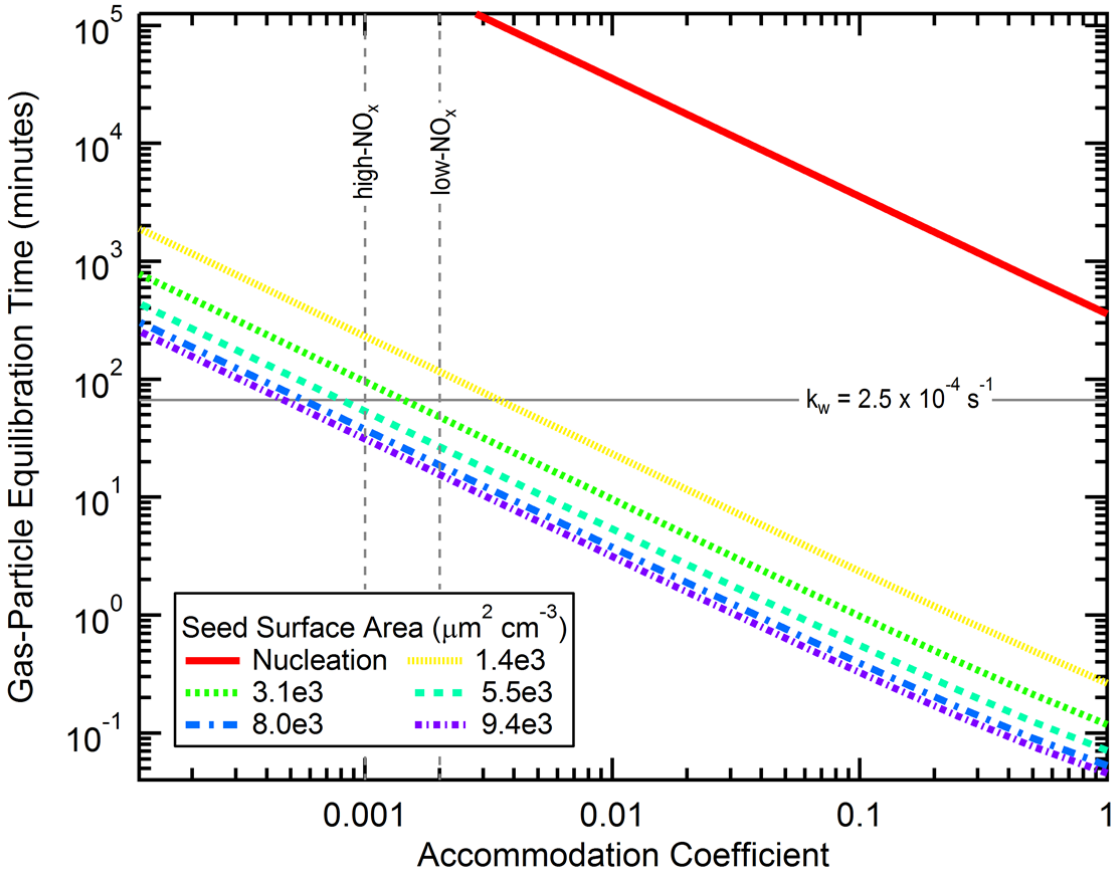

Fig. S5: Calculated gas-particle equilibration time as a function of the gas-particle mass accommodation coefficient, α, for different seed surface areas corresponding to the low-NO_x experiments. The horizontal gray line indicates the timescale associated with vapour wall-loss for k_w = 2.5 x 10^{-4} s^{-1}. The vertical dashed gray lines indicate the optimal values of α determined here for the high- and low-NO_x toluene systems. For the nucleation experiments, it is assumed that the particles are 10 nm diameter.

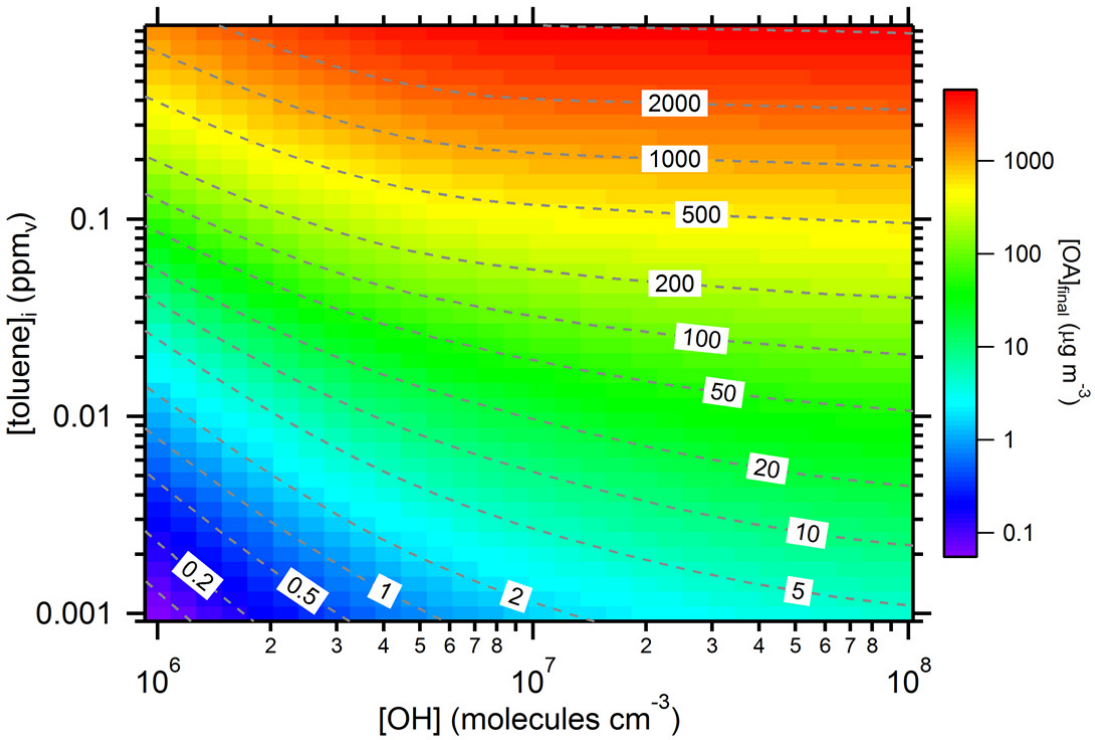

Fig. S6: Calculated end-of-experiment SOA mass concentrations corresponding to the results shown in Figure 3. The SOA concentration is shown as a function of initial toluene concentration and OH concentration when k_w = 2.5 x 10^{-4} s^{-1} and C_w = 10 mg m^{-3}. The SOA concentrations for a given [toluene] and [OH] are indicated by colors and contours. Results are based on the optimal fit of the SOM to the low-NO_x experiments.

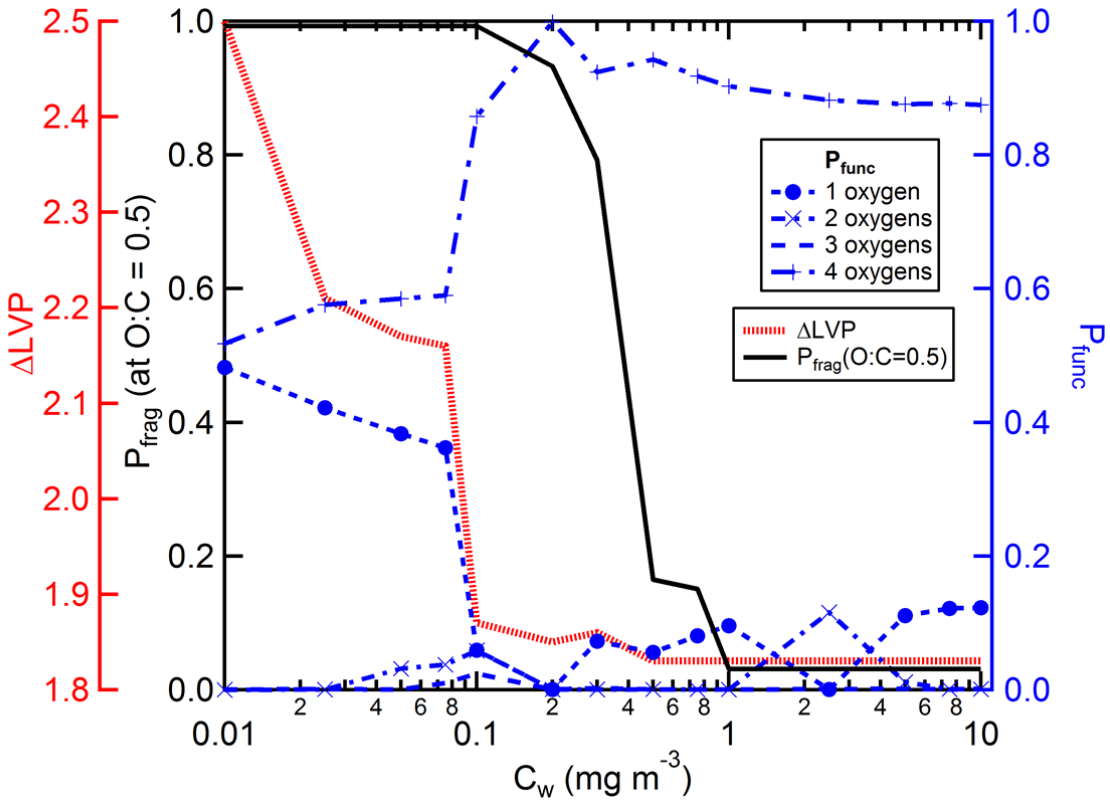

Fig. S7: The best-fit SOM parameters determined at each C_w corresponding to the results shown in Fig. 4 in the main text. The fragmentation probabilities, P_{frag}, were calculated from the best-fit m_{frag} values and Eqn. S3 using O:C = 0.5. ΔLVP corresponds to the decrease in vapor saturation concentration per oxygen added and P_{func} corresponds to the probability of adding 1, 2, 3 or 4 oxygen atoms per reaction.

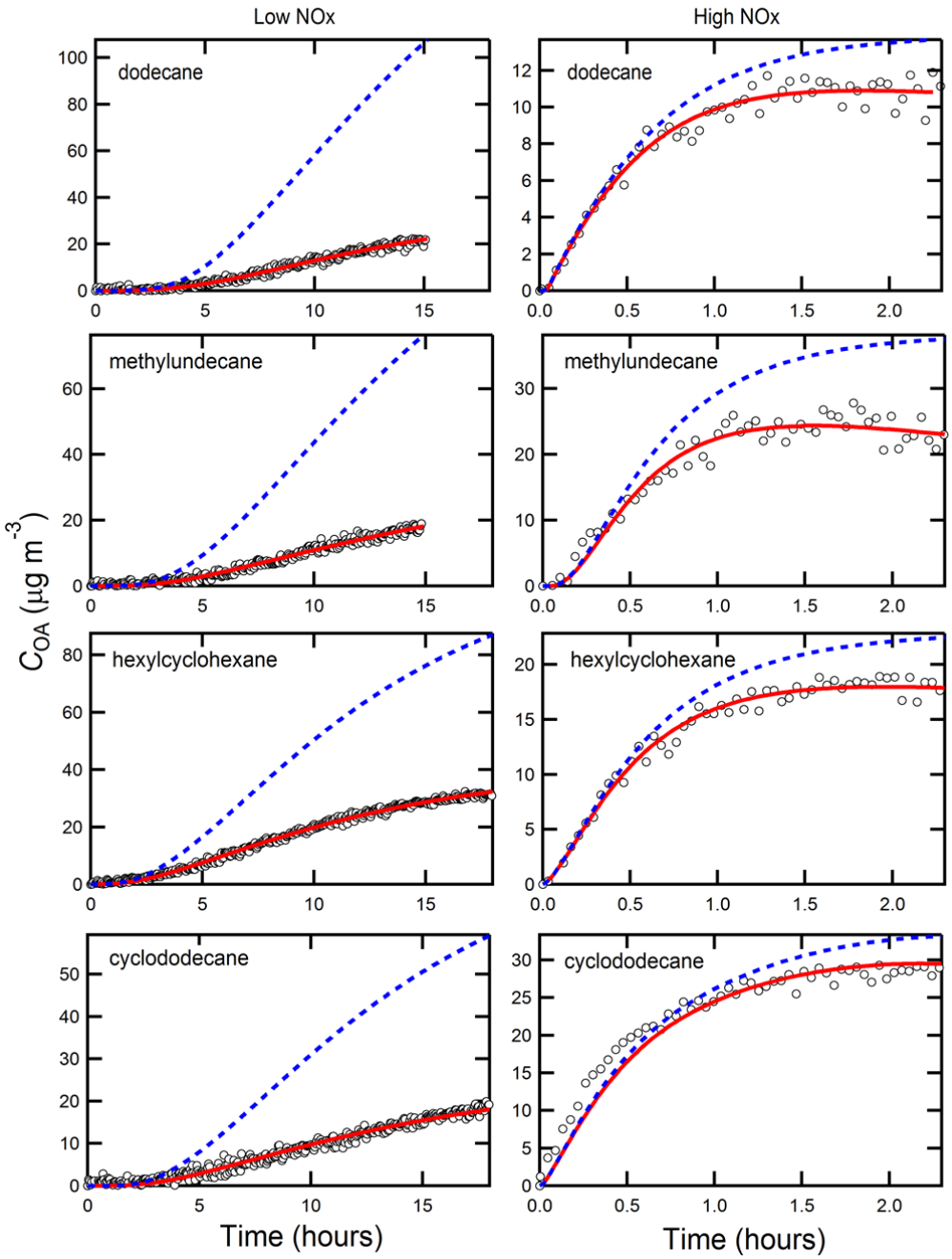

Fig. S8: Results from historical low (left panels) and high (right panels) NO_x SOA formation experiments for alkane photooxidation (open circles). The solid red lines are best-fit SOM results when wall losses are accounted for assuming that k_w = 1 x 10^{-4}, α = 1 and C_w = 10 μg m^{-3}. The blue dashed lines are the simulated SOA concentrations when wall-loss is turned off, but the SOM parameters determined from the best-fit with wall-loss on are retained.

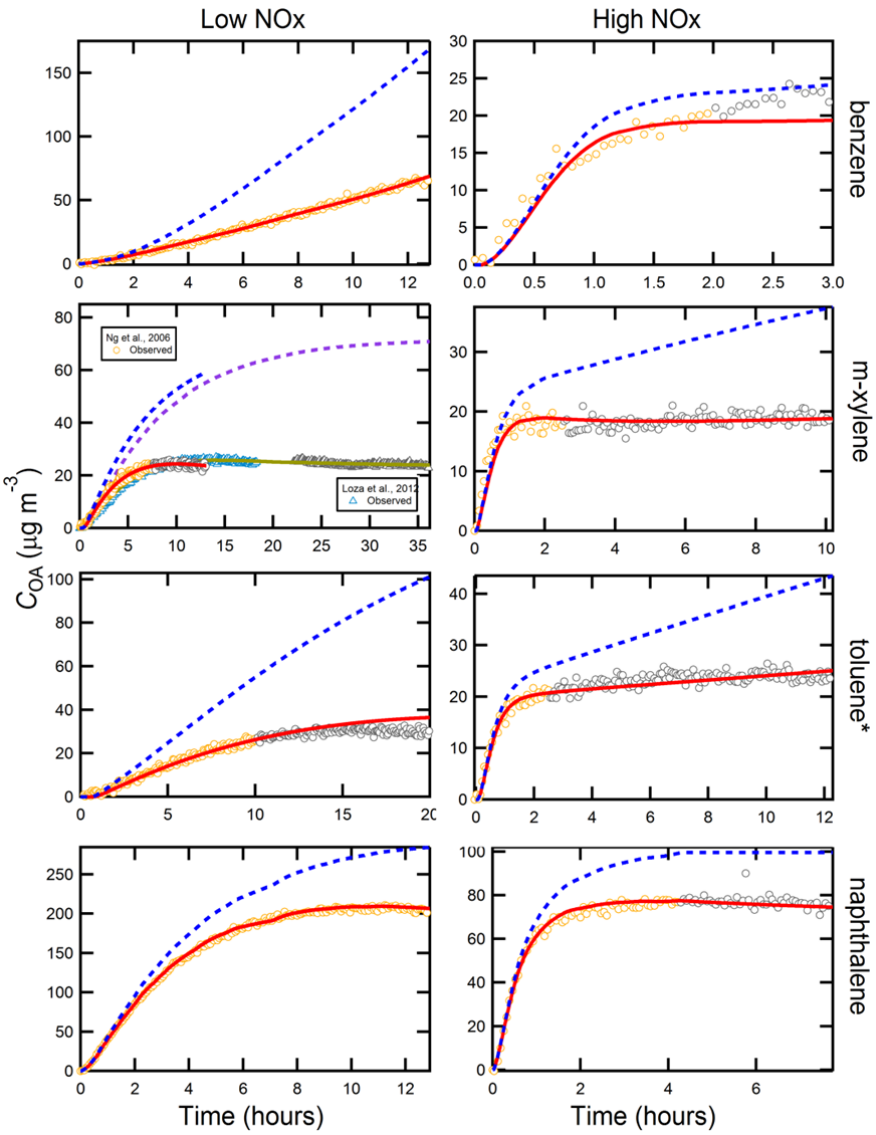

Fig. S9: Same as Fig. S3, but for aromatics. Importantly, the toluene experimental results are from Ng et al. (3), not from the current set of experiments. For each experiment, data collected over the full experiment time is shown. However, the SOM fitting has been restricted to the periods shown as colors other than gray (orange or blue). The gray points are data that were collected, but not used in fitting. These data have been excluded to be consistent with the range of data considered in Ng et al. (3) and Chan et al. (1), where 2-product fits have been performed. For m-xylene, low-NO_x, fits to data from Ng et al. (3) and Loza et al. (5) are shown separately.

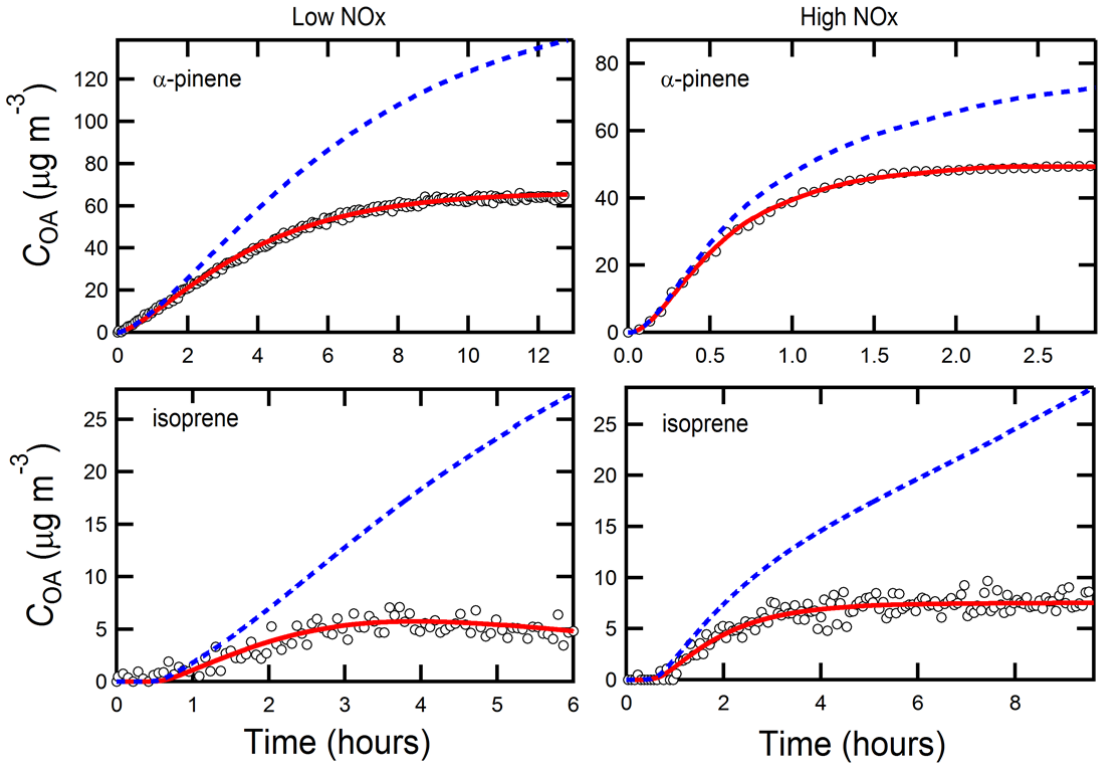

536

537 **Fig. S10:** Same as Fig. S8, but for α-pinene (4) and isoprene (4) photooxidation.

538

539

540

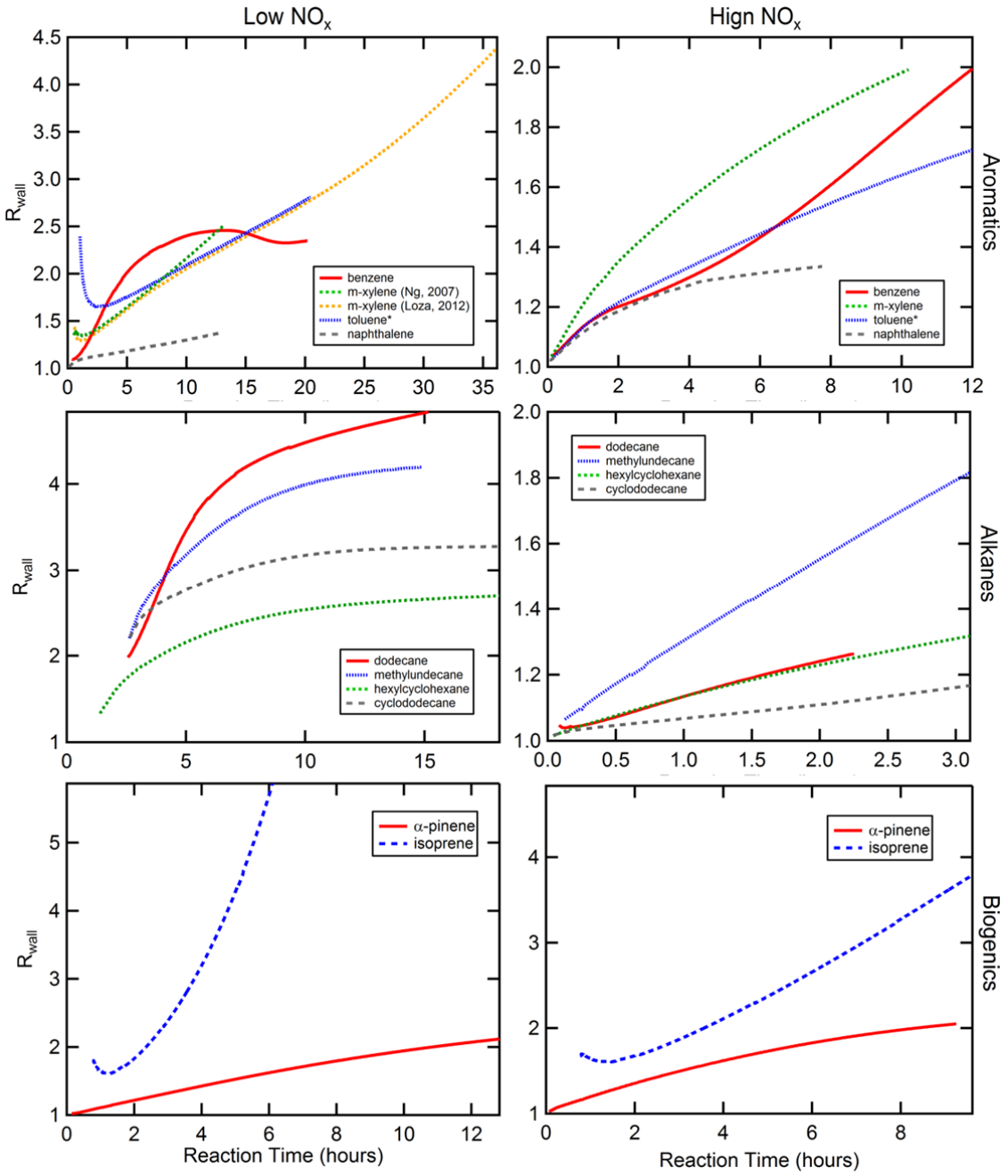

Fig. S11: Calculated time-dependent R_{wall} values for historical experiments based on the results shown in Fig. S8 - Fig. S10. Results are grouped according to species type and NO_x level. Left panels are low-NO_x and right panels high-NO_x results. Note that the toluene results in the top panels are based on data presented in Ng et al. (3), not from the current set of experiments. Results are shown for m-xylene, low-NO_x for two separate experimental data sets: Ng et al. (3) and Loza et al. (5). The presented results are limited to the period where $C_{OA} > 0.5$ µg m^{-3}.

Table S1. Experimental conditions for toluene SOA photooxidation experiments in the 24 m^3 Caltech chamber.

	Exp. (#)	$[HC]_0$ (ppb)	$[NO]_0$ (ppb)	$[NO_2]_0$ (ppb)	Initial [VOC]/[NO_x] (ppbC/ppb)	Additional NO injection	Initial seed surface area (μm^2 cm^{-3})	Initial surface area ratio (Aerosol/Wall)
High NO_x	1	~36.8	~ 19.0	~ 34.4	4.8	yes	~ 0	~ 0
	2	~38.7	~ 19.6	~ 32.2	5.2	yes	1.69×10^3	8.57×10^{-4}
	3	~37.9	~ 15.5	~ 34.9	5.3	yes	3.51×10^3	1.88×10^{-3}
	4	~37.9	~ 17.5	~ 31.7	5.4	yes	6.70×10^3	3.32×10^{-3}
	5	~38.2	~ 13.1	~ 31.5	6.0	yes	8.51×10^3	4.83×10^{-3}
	6	~38.7	~ 16.8	~ 35.3	5.2	yes	1.15×10^4	5.72×10^{-3}
Low NO_x	1	~33.9	< DL[c]	< DL	--	--	~ 0	~ 0
	2	~37.6	< DL	< DL	--	--	1.41×10^3	1.03×10^{-3}
	3	~37.3	< DL	< DL	--	--	3.10×10^3	2.13×10^{-3}
	4	~36.8	< DL	< DL	--	--	5.47×10^3	4.07×10^{-3}
	5	~38.7	< DL	< DL	--	--	7.95×10^3	5.17×10^{-3}
	6	~37.9	< DL	< DL	--	--	9.41×10^3	6.70×10^{-3}

[a] Detection limits (DL) for O_3, NO, and NO_2 are 0.5 ppb, 0.4 ppb, and 0.4 ppb, respectively.

Table S2. Conditions for low-NO_x experiments in the 28 m^3 Caltech chamber.

VOC	Ref	Date [mm/dd/yy]	$[VOC]_0$ (ppb)	$[NO_x]_0$ (ppb)	Initial [VOC]/[NO_x] (ppbC/ppb)	[OH][a] (molecules/cm^3)	% Yield at C_{OA} = 10 μg m^{-3}	k_{OH} (cm^3 $molecules^{-1}$ s^{-1})
n-dodecane	(6)	03/16/11	34.0	<2	--	$2.5x10^6$	6.1	$1.34x10^{-11}$
methylundecane	(6)	02/25/11	28.1	<2	--	$2.4x10^6$	7.2	$1.34x10^{-11}$
cyclododecane	(6)	02/23/11	9.8	<2	--	$2.7x10^6$	17.2	$1.34x10^{-11}$
hexylcyclohexane	(6)	03/21/11	15.6	<2	--	$3.0x10^6$	15.4	$1.34x10^{-11}$
benzene	(3)	11/04/06	414	<2	--	$3x10^6$	23.8	$1.22x10^{-12}$
toluene[c]	(3)	10/24/06	52.7	<2	--	$3.3x10^6$	26.7	$5.63x10^{-12}$
m-xylene[d]	(3)	10/27/06	19.3	<2	--	$3x10^6$	28.2	$2.31x10^{-11}$
m-xylene[d]	(5)	10/11/10	29.2	<2	--	$2.5x10^6$	21.4	$2.31x10^{-11}$
naphthalene	(1, 2)	08/13/08	31.5	2	--	$2x10^6$	19.0	$2.44x10^{-11}$
α-pinene	(4)	06/02/10	66.2	<2	--	$3x10^6$	36.8	$5.3x10^{-10}$
isoprene	(4)	02/25/09	49	<2	--	$2x10^6$	4.3[b]	$1x10^{-10}$

[a] Average over the experiment
[b] Maximum yield, since maximum C_{OA} < 10 μg m^{-3}.
[c] From historical experiments by Ng et al. (2007), not the current set of experiments.
[d] m-xylene data are available from two independent sets of experiments.

Table S3. Conditions for high-NO_x experiments in the 28 m^3 Caltech chamber.

VOC	Ref.	Date [mm/dd/yy]	$[VOC]_0$ (ppb)	$[NO]_0$ & $[NO_2]_0$ (ppb)	Initial $[VOC]/[NO_x]$ (ppbC/ppb)	$[OH]$[a] (molecules/cm^3)	% Yield at C_{OA} = 10 μg m^{-3}	k_{OH} (cm^3 $molecules^{-1}$ s^{-1})
n-dodecane	(6)	05/12/11	32.2	343/--	1.13	$4.5x10^7$	6.2	$1.34x10^{-11}$
methylundecane	(6)	03/01/11	72.4	366/--	2.37	$3.3x10^7$	5.1	$1.34x10^{-11}$
cyclododecane	(6)	05/23/11	13.8	362/--	0.46	$2.7x10^7$	38.3	$1.34x10^{-11}$
hexylcyclohexane	(6)	03/22/11	22.1	320/--	0.83	$4.1x10^7$	12.3	$1.34x10^{-11}$
benzene	(3)	01/15/07	336	83/86	11.9	$3.2x10^7$	15.6	$1.22x10^{-12}$
toluene[c]	(3)	10/14/06	138	373/568	1.03	$3.6x10^7$	8.3	$5.63x10^{-12}$
m-xylene	(3)	10/05/06	89.8	469/474	0.76	$4.2x10^7$	3.9	$2.31x10^{-11}$
naphthalene	(1, 2)	08/14/08	48.6	404/171	0.85	$2.5x10^7$	11.2	$2.44x10^{-11}$
α-pinene	(4)	06/03/10	44.9	446/398	0.53	$1.4x10^7$	9.5	$5.3x10^{-11}$
isoprene	(4)	04/04/09	268	535/402	1.43	$6.6x10^6$	1.0[b]	$1x10^{-11}$

[a] For all high-NOx experiments HONO was used as the OH source. The [OH] was not constant in time, but decreased rapidly from the start of the experiment by at least an order of magnitude. The [OH] derived from the first [VOC] measurement after the lights were turned on is given here.
[b] Maximum yield, since maximum C_{OA} < 10 μg m^{-3}.
[c] From historical experiments by Ng et al. (2007), not the current set of experiments.

Table S4. Derived SOM parameters for the experiments when vapor wall-loss is accounted for (assuming C_w = 10 μg m^{-3}).

VOC[a]	Fragmentation	ΔLVP	P1	P2	P3	P4	χ^2_{red} [b]
		Low NO_x					
toluene (this study)	5	1.83	0.123	0.001	0.002	0.875	1.74
n-dodecane (6)	0.671	1.58	0.977	0.016	0.003	0.004	1.47
methylundecane (6)	0.433	1.92	0.997	0.000	0.001	0.002	1.33
cyclododecane (6)	1.56	1.90	0.994	0.000	0.001	0.005	1.73
hexylcyclohexane (6)	0.78	1.84	0.885	0.106	0.001	0.008	0.56
benzene[c] (3)	0.01	2.29	0.284	0.000	0.644	0.072	0.42
toluene[c] (3)	0.01	1.88	0.001	0.001	0.727	0.271	1.36
m-xylene[c] (3)	0.245	1.96	0.000	0.085	0.836	0.079	0.57
m-xylene[c] (5)	0.069	1.88	0.285	0.000	0.613	0.101	0.20
naphthalene (1, 2)	0.072	1.76	0.382	0.027	0.431	0.161	0.04
α-pinene (4)	0.151	1.91	0.262	0.619	0.075	0.044	0.19
isoprene (4)	0.01	2.23	0.000	0.146	0.826	0.028	1.61
		High NO_x					
toluene (this study)	1.02	1.42	0.000	0.000	1.000	0.000	1.10
n-dodecane (6)	0.188	1.45	0.963	0.000	0.001	0.036	0.07
methylundecane (6)	0.188	1.12	0.263	0.277	0.455	0.005	0.61
cyclododecane (6)	0.01	1.69	0.664	0.002	0.004	0.33	0.64
hexylcyclohexane (6)	0.153	1.75	0.832	0.086	0.055	0.028	0.14
benzene[c] (3)	0.912	1.47	0.105	0.001	0.893	0.001	1.15
m-xylene[c] (3)	0.18	1.54	0.000	0.000	1.000	0.000	0.64
toluene[c] (3)	0.039	1.46	0.001	0.001	0.906	0.094	1.13
naphthalene[c] (1, 2)	0.64	1.41	0.835	0.001	0.002	0.162	0.17
α-pinene (4)	0.080	1.81	0.193	0.694	0.101	0.012	0.04
isoprene (4)	0.322	2.23	0.679	0.321	0.000	0.000	0.79

[a] The toluene experiments from this study were conducted in the 24 m^3 Caltech chamber (i.e. "new" experiments) and simulated using k_w = 2.5 x 10^{-4} s^{-1} and the experimentally-determined optimal α (~2 x 10^{-3}). All other experiments, including the toluene experiments from (3) were conducted in the 28 m^3 Caltech chamber (i.e. "historical" experiments") and simulated using k_w = 1 x 10^{-4} s^{-1} and α = 1.

[b] The reduced χ^2 associated with the best fit.

[c] Fits were performed over the ranges shown in Fig. S9.